**Seasonal comparisons of GEOS-Chem-TOMAS (GCT) simulations with AERONET-inversion retrievals over sites in the North American and European Arctic**

**Y. AboEl-Fetouh[1], N. O'Neill[1], J.K. Kodros[2], J.R. Pierce[2], H. Lu[3], K. Ranjbar[1], and P. Xian[4]**

1 CARTEL, Université de Sherbrooke, Sherbrooke, Québec, Canada

2 Colorado State University, Fort Collins, Colorado, USA

3 Compute Canada/Quebec, Université de Sherbrooke, Québec, Canada

4 Marine Meteorology Division, Naval Research Laboratory, Monterey, CA, USA

# Key Points

1. Fine mode effective radius was systematically underestimated by GCT. This was likely due to underestimated smoke particle size.
2. GCT captured the springtime coarse mode particle size distribution peak of the climatology as well as a weak but systematic fall increase.
3. GCT captured most fine and coarse mode seasonal aerosol trends previously observed in a climatology of Arctic AERONET sites.

# Abstract

GEOS-Chem TOMAS (GCT) simulations of AERONET-inversion products during 2015 were compared with AERONET-inversion products from the multi-year climatology of Aboel-Fetouh et al. (2020) (AeF) and for year 2015 acquired over 5 stations in the North American and European Arctic. The GCT simulations of particle size distributions (PSD) did not capture a spring to summer radius increase of the fine mode (FM) peak observed by AeF but did capture AeF's springtime coarse mode (CM) peak (small-sized CM peak with a radius ~ 1.3 µm) and a weak late summer / fall increase in the amplitude of that peak. The lack of a spring to summer FM radius increase was likely due to the large GCT cell size (4° x 5°) and associated difficulties in the modelling of coagulation-induced smoke particle size. Conversely, the GCT simulation of the small-sized CM peak indicated a successful capture of the springtime influx of Asian dust. The fall increase of that GCT peak was associated with an increase of a larger (4 -7 µm) PSD mode that AeF suggested was due to local dust. GCT captured the seasonal (climatological-scale) FM AOD trend, the decreasing CM AOD trend, and the increasing trend of the FM fraction. The GCT CM AOD also showed a fall increase that was coherent with the increase of the simulated small-sized CM peak and with a lesser rate of decrease of the AeF CM AOD. Large GCT deviations from the AERONET retrievals were attributed to an extreme July, 2015 forest fire event.

# 1.Introduction

The importance of studying the impacts of aerosol radiation (direct effect) and aerosol cloud interaction (indirect effect) on climate change is well established (see Boucher et al.,2013). The climate forcing of aerosols over the Arctic is of particular importance due, notably, to climate feedback effects that result in Arctic amplification. Arctic aerosols are of local and remote (long-range transport) origins (see, for example, Hirdman et al., 2010). Their direct and indirect climate forcing role depends on their quantity independent (intensive) properties of chemistry, size and shape and quantity dependent (extensive) properties such as number, volume, or mass concentration: these properties are intrinsically related to the nature of the emission sources and the transport pathways into the Arctic.

Chemical transport models (CTMs) coupled with aerosol microphysics / chemistry packages are essential tools for understanding the dynamics of Arctic aerosols. However, modellers are faced with various challenges: for example, in the goal of rendering these models computationally fast there is a tendency to oversimplify their physical and chemical schemes. Table 1 of Schmale et al. (2021) presents a concise list of model deficiencies (as well as major measurement deficiencies) in simulating Arctic processes for aerosols of both local and long-range origin. The modelling deficiencies include the microphysics and chemistry of marine aerosols, the modelling of wet and dry deposition of aerosols during their transport, inadequate parameterizations of aerosols acting as INPs (ice nucleating parcels) and cloud / fog processing of aerosols. An important consideration in that paper was that (spatial/temporal) model resolutions were generally too coarse to capture particle formation mechanisms, the physical and chemical processing of aerosols and aerosol cloud interaction in general. The required model resolution and its degree of sophistication in simulating optical and microphysical aerosol dynamics is a trade-off that depends on the resolution of a given process as well as the type and resolution of the aerosol measurement being simulated.

The process of increasing the accuracy of the aerosol schemes employed in CTMs will augment the understanding of aerosol processes (including sources and composition) and forecasting abilities. The most comprehensive approach to improving model accuracy is to compare CTM simulations with columnar products of robust, $1^{st}$ order, vertically integrated or vertically averaged aerosol parameters: parameters that models must satisfy before one can aspire to assess their simulation performance with respect to more $2^{nd}$ order products at, for example, a single altitude. The Aerosol Robotic Network (AERONET) is a global network of ground-based sunphotometer/sky radiometer instruments that provide long-term retrievals of columnar aerosol products (over periods that range up to 20 years for the AERONET sites in the Arctic). The availability of these retrieval products enables the generation of robust climatological-scale databases that can form the basis of comparisons with CTM simulations.

AERONET "ground-truth" retrievals have been widely used in comparisons with satellite retrievals and model simulations. Hesaraki et al. (2017) provided a summary of model comparisons with Arctic AOD and Angstrom parameter retrievals: the performance of the models could be generally characterized as good to marginal with respect to the simulation of both parameters. Breider et al. (2014) found reasonable agreement between Goddard Earth Observing System chemical-transport model (GEOS-Chem) simulations of climatological-scale AERONET/AEROCAN[1] AODs. Hesaraki et al. (2017) showed that springtime CM (coarse mode) AOD peaking due to Asian and/or Saharan dust and FM (fine mode) AOD peaking due to Arctic haze were approximately captured by GEOS-Chem. They also observed that FM AOD and CM AOD log-space histograms were better representations than linear-space histograms of the measured and modelled retrievals[2] (with attendant implications, for example, on the correlation coefficients of the simulations versus the retrievals).

The standard GEOS-Chem aerosol scheme (bulk model) is based on prescribed particle size distributions (PSDs) of speciated, externally mixed (independent), aerosol populations (with the exceptions of sea spray and dust, with 2 and 4 size bins, respectively). Bulk models do not incorporate aerosol microphysical processes that depend on the form of the PSD (nucleation and coagulation are examples of such processes). In contrast, the "TwO Moment Aerosol Sectional" (TOMAS) microphysical package (Adams & Seinfeld, 2002) simulates a 40-bin (sectional) PSD with two moments (aerosol mass and number). The integration of TOMAS into GEOS-Chem is known as GEOS-Chem-TOMAS (hereafter referred to as GCT).

GCT has been used to gain insight into a variety of aerosol processes in the Arctic. These studies include (1) the drivers of new particle formation (Croft et al., 2016a) (2) the season cycle of Arctic PSDs (Croft et al., 2016b) , (3) the role of marine organic species in shaping the Arctic PSDs (Croft et al., 2019), (4) Arctic black carbon mixing state (Kodros et al., 2018), and (5) the vertical profile of Arctic aerosol absorption and scattering (Leaitch et al., 2020). While GCT was evaluated using in situ measurements in each of these Arctic-focused studies, it has not been evaluated with the comprehensive suite of columnar optical and microphysical properties that can be derived from the ground-based remote sensing of spectral AOD and almucantar radiance measurements: specifically the AERONET optical and microphysical inversions (Dubovik & King, 2000 , Sinyuk et al., 2020).

In this paper, we compare GCT simulations with ground-based AERONET sunphotometer/almucantar radiometer inversions acquired over five Arctic stations (AboEl-Fetouh et al., 2020; hereafter AeF). We specifically compare seasonal (climatological-scale) variations of a number of key parameters: PSDs and the

[1] AEROCAN is the federated Canadian subnetwork of AERONET. From this point on we will, for the sake of simplicity, just refer to AERONET

[2] A finding that was validated for total AOD on a global scale (for AERONET and satellite retrievals) by Sayer & Knobelspiesse (2019).

radius position of certain seasonal and species dependent aerosol features along with key optical and microphysical parameters. These latter parameters include fine and coarse mode (FM and CM) AOD, FM and CM effective radii, and FM fraction (FMF) (defined in AeF). The seasonal AERONET parameters are compared with a single year of GCT simulations (2015). In doing so we evaluate GCT by comparing its single-year predictions within the envelope of a multi-year AERONET climatology as well as with AERONET retrieval parameters acquired specifically in the simulation year of 2015. This process enables a better understanding of the robustness of seasonal variations derived from the AERONET retrievals and how well GCT simulations can be employed to predict these (climatological-scale) variations across the Arctic. In addition, an analysis of the departures from seasonal variations by both the AERONET retrievals and GCT simulations informs our understanding of the optical and microphysical dynamics of those departure events.

# 2.AERONET retrievals and models

## 2.1 AERONET inversions

AeF employed climatological-scale (monthly binned), Version 3, Level 1.5 AERONET inversions from six AERONET sites in the North American and European Arctic. Microphysical and optical parameters of an extensive-parameter nature were reported in terms of geometrical means and standard deviations while intensive-parameter properties such as effective radius, and semi-intensive parameters, such as the FMF, were reported in terms of arithmetic means and standard deviations. The AERONET optical parameters were interpolated to 550 nm to match the typical wavelength of the aerosol modelling community. Further details on the choice of statistical measures, the choice of AERONET product level, the interpretation of the seasonal trends and multi-year histograms can be found in AeF.

The five AERONET stations employed in this study are: 1) Barrow, Alaska, USA, 2) Resolute Bay, Nunavut, Canada, 3) PEARL-Eureka, Nunavut, Canada, 4) Thule, Greenland, Denmark, and 5) Hornsund, Spitsbergen, Norway. Details on the latitude, longitude and elevation of each station are given in Table 1 of AeF along with their MYSP (the multi-year sampling period over which their aerosol climatologies were derived). Details on the reasons for the selections of these stations are also outlined in AeF.

## 2.2 Modelling considerations

The TOMAS aerosol microphysics scheme was originally described in Adams & Seinfeld (2002). Its coupling to GEOS-Chem is originally described in Trivitayanurak et al. (2008), and the specific model setup and emissions used here are described in Kodros and Pierce (2017). In this work, we use GEOS-Chem version 10.01 (further details can be found here: https://geos-chem.seas.harvard.edu/ ).

The model is driven by MERRA-2 (second Modern-Era Retrospective analysis for Research and Applications) assimilated meteorology (Gelaro et al., 2017). The latitude/longitude grid size is 4° x 5° with 47 vertical levels up to 0.01 hPa: for the purposes of our columnar analysis, we focussed on the lower 30 layers, up to ~250 hPa (around 10 km). Aerosol mass and number concentrations were recorded every 6 simulation hours.

The TOMAS module in GCT is a comprehensive aerosol microphysics model that explicitly simulates PSD evolution by condensation, coagulation, nucleation, size-dependent emissions, and size-dependent deposition. In contrast, simpler bulk aerosol schemes tend to make PSD and aerosol mixing simplifications for reasons that are often related to operational considerations (see, for example, the sectional vs bulk PSD analysis of cloud-condensation-nuclei impact carried out by Kodros & Pierce (2017) for a comparison of the impacts of the two types of models). GCT tracks total particle number and speciated particle mass (i.e. the output of the model at any given time, grid cell and vertical layer is total particle number and speciated mass) across 40 size bins with dry bin radii ranging from approximately 0.0005 µm to 5 µm. Within each size bin, all species except black carbon are assumed to be internally mixed (multi-species particles) while black carbon is externally mixed.

Mie (spherical-particle) optical theory (see, for e.g., Bohren & Huffman, 2004) was employed to calculate 550 nm AODs offline ("offline" in the sense that the speciated mass of any given radius bin at any given grid cell was transformed, post GCT simulation, into radius and refractive index inputs required by the Mie program). The real and the imaginary parts of the refractive indices (n and k) and the densities of the pure GCT aerosol types are listed in Table 1. The assumed n and k values for each species must be weighted by the species volume-fractions to obtain composite n and k value for the mixture in any given GCT grid cell at any given simulation time (see Lesins et al. (2002) and Curci et al. (2015) for a general optical discussion on mixed aerosol components).

@ >p(- 8) * >p(- 8) * >p(- 8) * >p(- 8) * >p(- 8) * @ **Aerosol Type** & **n** & **k** & **Density**

**(kg/m$^3$)** & **Reference for density**
Water (H2O) & 1.33 & 1.96E-9 & 1000 &

- 

Sulphate (SO4) & 1.43 & 1.00E-8 & 1780 & Tang (1996)
Sea-salt (SS) & 1.50 & 1.00E-8 & 2165 & Tang (1996)
Black Carbon (BC) & 1.95 & 0.79 & 1800 & Bond & Bergstrom (2006)
Organic Carbon (OC) & 1.53 & 6.00E-3 & 1400 & Dick et al. (2000)
Dust & 1.53 & 5.50E-3 & 2650 & Tegen & Fung (1994)

Table 1 Nominal values of the mass density as well as the 550 nm values of the

real and imaginary parts of the refractive index employed to characterize GCT aerosol types.

The coarse TOMAS spatial resolution of 4° x 5° that we employed in the context of this paper is limited in its capacity for monitoring high frequency aerosol events in the spatial and temporal domain. It is better suited to climatological scale comparisons with AeF's detailed, multi-parameter seasonal climatology. The GCT ingestion of smoke emission information from satellite hot-spot retrievals is dynamic but of relatively low frequency (daily temporal resolution). As a means of better understanding significant event-level departures of GCT from AeF's seasonal climatology (specifically for a 2015 case of high frequency smoke intrusions into the Arctic), the Navy Aerosol Analysis and Prediction system (NAAPS) model was employed to simulate speciated 550 nm AODs at a relatively high spatial resolution (1° x 1°). NAAPS is a global aerosol transport model which simulates four externally mixed species of aerosols (FM smoke, FM anthropogenic and biogenic aerosols, CM dust and CM sea salt). It uses bulk microphysics in order to achieve fast (operational) computational times. The NAAPS reanalysis version that we employed in this study (the NAAPS-RA model described by Lynch et al., 2016) assimilates quality controlled (550 nm) MODIS-retrieved AODs. At sub-Arctic latitudes, NAAPS-RA benefits from a rapid sampling of biomass burning (MODIS hot-spot) emission sources (hourly database) coupled with assimilated MODIS AODs that are significantly more spatially comprehensive than those acquired over the Arctic. The underlying meteorology that drives NAAPS also incorporates meteorological observations through data assimilation at its analysis time. More information on NAAPS-RA can be found in the supplementary material.

# 3. Methodology

## 3.1 On the general nature of our GCT vs AERONET comparisons

AERONET does not provide speciated aerosol products. However, as pointed out by AeF, the algorithmic division into FM and CM aerosols is a form of speciation since the formation and transportation mechanisms governing aerosol dynamics is very much bimodal in nature. This bimodality feature provides a basis for investigating the extensive and intensive parameters of interest from both the ground-based retrievals and model simulations (AeF) .

The approach taken in this comparison analysis was to contextualize the 2015 GCT simulations (and the 2015 AERONET retrievals) in terms of the MYSP climatological-scale findings of AeF: namely the seasonal, monthly-binned trends of the fundamental FM and CM retrieval parameters of the AERONET inversion. We then analysed the similarities-to or departures-from the climatological-scale seasonal MYSP results. In the case of significant departures, we performed more detailed investigations of the 2015 retrievals and simulations in order to

better understand the reasons for those departures. The underlying rationale for this approach is that GCT, even GCT constrained to a single year, can largely simulate the seasonal (climatological-scale, month to month) variations of a variety of optical and microphysical, extensive, and intensive parameters acquired by the AERONET extinction/sky radiance retrievals.

It must be emphasized that the number of per-month AERONET retrievals are typically small[3] (notably in the case of one single year of retrievals). A threshold of 10 retrievals per month was (somewhat) arbitrarily set for admissible monthly averages (thus, for example, only Thule had a sufficient number of retrievals to pass the 10-retrieval threshold for the month of April 2015). That threshold aside, the small-N (small sample number) AERONET statistics of 2015 (see the AERONET-inversion retrieval numbers for 2015 in the legends of Figure 1) are generally expected to be at the margins of significance (Barrow, for example, shows no month with higher than 23 retrievals).

The AERONET Level 1.5 inversion products are cloud screened. GCT simulations can be processed through a crudely analogous filtering process wherein simulation points of a certain relative humidity (RH) threshold are excluded from the monthly averaged statistics. As a check on the statistical impact of this GCT "cloud screening" process we compared monthly "cloud screened" FM and CM AOD GCT averages with the standard monthly averages that were free of any RH filtering (the results, discussed below, employed a RH threshold of 95%). The temporal irregularity of AERONET retrievals can have an effect on comparisons between the GCT and AERONET averages of 2015. We tested this potential source of sampling bias below by limiting GCT FM and CM AODs admissible to the monthly averaging to times that were synchronized to AERONET retrieval times (where "synchronized" refers to AERONET retrievals being within ±3 hours of the nominal GCT times).

Finally, we note that while AERONET bins have fixed radii, the exact GCT bin radii are dynamic: bin radii depend on mass to radius conversion factors (including the contribution of RH-driven aerosol water uptake) in each grid cell of the simulation domain. Practically, this means variations in radius bin centers of $<\sim 1\%$ at the smallest radii to $<\sim 5\%$ at the largest radii (from computations of the coefficients of variation computed for all stations and all months of the 2015 simulation).

## 3.2 Aerosol parameters and their comparison protocols

The AERONET-derived, monthly-binned parameters that we employed were the arithmetically averaged PSD, the 550 nm geometric means and geometric standard deviations of the FM and CM optical depths ($_{f,g}$, $_{f,g} \times \mu_f^{\pm 1}$ and $_{c,g}$, $_{c,g} \times \mu_c^{\pm 1}$) the arithmetic means and standard deviations of the FM and CM effective radii ($<r_{eff,f}> \pm$ $(r_{eff,f})$ and $<r_{eff,c}> \pm$ $(r_{eff,c})$) as well as the

[3] within a context of the retrieval histogram of a given month being representative of its large-N probability distribution.

550 nm FMF (details on the climatological-scale MYSP statistical approach for deriving monthly-binned averages can be found in AeF). Implicit in this choice of parameters is the question of the opto-physical significance of any given retrieval parameter: this is intrinsically related to the trade-off between a finer (high order) choice of parameters (i.e. "order" in the sense of a Taylor series function of the dependent parameters of wavelength and almucantar angle) and the level of significance that one can aspire to from the AERONET retrievals given the typical errors in spectral AOD and almucantar radiance. The FM / CM characterization is, for typical AOD and almucantar radiance accuracies, essentially a low order type of retrieval (see, for example Table 1 of O'Neill et al. 2003). We, nonetheless, also considered details of the full-fledged PSD retrieval product in order to investigate the possibility of higher order sensitivities.

We derived off-line GCT parameters analogous to all the AERONET retrieval parameters and then computed monthly binned analogues to the monthly binned AERONET retrievals defined in the previous paragraph. As part of the comparison protocol, we defined a FM versus CM cut-off radius that simulated as nearly as (practically) possible the cut-off radius of the AERONET processing stream. That cut-off radius was taken as the minimum of the retrieved particle-volume size distribution retrieval where the minimum is limited to four prescribed bin-center choices (approximately 0.439, 0.576, 0.756 and 0.992 µm). We chose the average AERONET-derived, station-dependent cut-off radius for each month.

AERONET PSDs are retrieved over 22 equally spaced logarithmic bins (Dubovik et al., 2002) while the GCT bin radii, as noted above, vary by a small percentage. A more substantive element in the PSD comparisons is that the AERONET radius bin-center range extends up to 15 µm whereas the center of the largest GCT bin is only ~4.5 µm. At the lower end of the radius scale, GCT extends an order of magnitude below the AERONET PSD retrieval range. When deriving bin constraints analogous to AERONET, we simply cut off the GCT range at the AERONET minimum (lowest bin edge of 0.04 µm radius as per Table S1.2 in the supplementary material). At the upper radius range, we excluded AERONET bins of bin-centre radius greater than 4 µm when calculating $r_{eff,c}$ from the AERONET PSD retrievals.

The fixed temporal sampling resolution of the GCT simulations produces 4 points per day or 120 points per 30-day month. In contrast, the AERONET sampling rate is nominally higher (once per hour) but, because of cloud obscuration, light-season limitations and other sampling constraints, it is very irregular (to the extreme limit of the polar night for the high Arctic stations when there are no retrievals from late September to late March).

# 4.Results

## 4.1 PSD comparisons

Figure 1 shows AERONET PSDs (left column) vs GCT simulations (right column) for 2015 (the MYSP PSDs of AeF were excluded, for the sake of simplicity, in this one case). The AERONET admissibility threshold of 10 retrievals can significantly curtail the seasonal extent of the 2015 results (to the point, for example, that only Thule statistics were admissible for the month of April).

AeF reported a systematic spring to summer increase in the radius of the FM peak over the MYSP of all stations (except Resolute Bay). They attributed this increase to the seasonal transformation from a dominance of smaller FM Arctic haze aerosols in the spring to a dominance of larger FM smoke aerosols in the summer. The retrieved 2015 AERONET PSDs of Figure 1 generally show a similar spring to summer FM increase (see, respectively, the grey and dark-grey dashed vertical lines superimposed on the May and July peaks) as that reported by AeF[4]. The singular month of August at Resolute Bay, PEARL and Thule did not follow this Figure 1 trend (while the trend at Hornsund could not be evaluated given only two months of admissible retrievals). GCT shows no significant spring to summer increase in the radius of the FM peak: a null result that was, at least, in part due to GCT underestimating smoke particle size (see Sections 4.2.1 and 4.3.1 below). The AERONET retrievals and the GCT simulations both show the general maximum amplitude of the FM peak in July[5] (the results of an extreme July smoke event as we discuss below).

All AERONET stations capture the April/May component of the springtime CM peak at 1.3 µm (peak that AeF attributed to Asian dust) while also capturing a June peak whose radius position is more variable than the (largely 1.3 µm) "weaker amplitude peak in June" reported by AeF. The capture of peak springtime bin-center values from 1.2 to 1.5 µm by GCT is roughly in agreement with the Asian dust peak of the AERONET retrievals.

A second set of 2015 AERONET peaks from ~ 3 to 7 µm in July and/or August for all stations is roughly coherent with the ~ 4 to 7 µm[6] late summer and early fall CM peaks reported by AeF[7]. They argued that an increase in the amplitude of the 4 to 7 µm CM peaks might be attributable to an increasing influence of wind-induced sea-salt and / or local dust aerosols. They also noted that local dust might represent the key influence since sea-salt particle sizes (estimated to be in the 2 – 4 µm volume-mean-radius range) were at the lower margin of

[4]who reported increases from .04 to 0.08 m from a springtime value close to 0.15 m

[5]The word "amplitude" is used frequently below. With respect to the PSD of Figure 1, we mean the magnitude of some dV/dlogr feature (notably associated with some modal peak)

[6]There is an incoherence in AeF wherein the peak range is sometimes referred to as "5–7 m" and sometimes "4 to 7 m". We retained the more general 4 to 7 m AeF range for use in the current paper.

[7]the increase (noted by AeF) in the amplitude of that feature from July to August for Barrow, Resolute Bay and Hornsund is inconclusive for the 2015 retrievals with only Resolute Bay having a (marginally) significant number of retrievals

the 4 to 7 µm peak. Ongoing, local-dust investigations of AERONET PSDs, supported by microphysical PSDs and lidar at the 0PAL Eureka site suggest that a (very flat) local dust peak occurs at a radius ~ 3 – 6 µm during July and August (co-author K. Ranjbar).

The lack of such a 4 to 7 µm peak in the GCT PSDs as well as their tendency (unlike the 3 to 7 µm AERONET peaks) to rapidly decrease in amplitude as the season progresses merits further comment. The spring to summer amplitude decrease of the GCT CM peaks is coherent with the amplitude decrease of the 1.3 µm (Asian dust) AERONET peaks of AeF and with the AERONET retrievals of 2015 for certain stations (namely Barrow, PEARL, and Thule; the decrease is of marginal significance for Hornsund and does not exist for Resolute Bay). The decreasing-amplitude trend of the GCT peaks goes through a noteworthy reversal with an amplitude increase at all stations in September (as well as an apparently modest increase in the radius position of the GCT peak at Barrow and Hornsund in August). These fall (late summer) increases in the amplitude or position of the GCT peaks suggest a GCT sensitivity to the increasing amplitude of winds (and thus wind-generated sea-salt and/or local dust) in the fall (late summer)[8] with a limitation to small-sized CM particles (the CM peak of 1.2 to 1.5 µm radius noted above coupled with the modal extent of that feature). We will return to a discussion of those moderate increases in the sections on the seasonal variation of the CM AOD and effective radius below.

[8]see, for example, the iconic high- and low-wind soil plot (Figure 11) of Sirois & Barrie, 1999 and AeF's GEOS-chem-generated seasonal plot (Figure 1b) of salt and dust (CM) AOD.

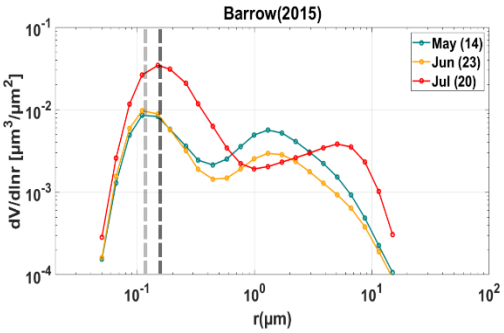
Barrow(2015)
May (14)
Jun (23)
Jul (20)
dV/dlnr [μm³/μm²]
r(μm)

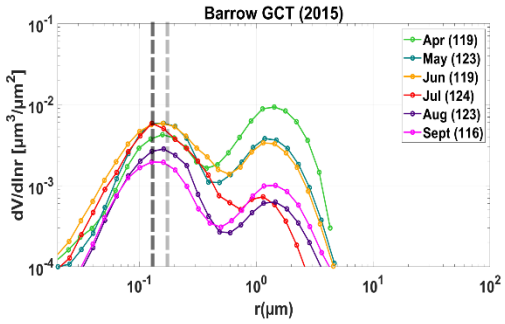
Barrow GCT (2015)
Apr (119)
May (123)
Jun (119)
Jul (124)
Aug (123)
Sept (116)
dV/dlnr [μm³/μm²]
r(μm)

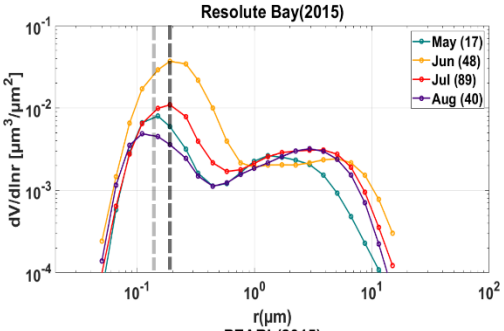
Resolute Bay(2015)
May (17)
Jun (48)
Jul (89)
Aug (40)
dV/dlnr [μm³/μm²]
r(μm)

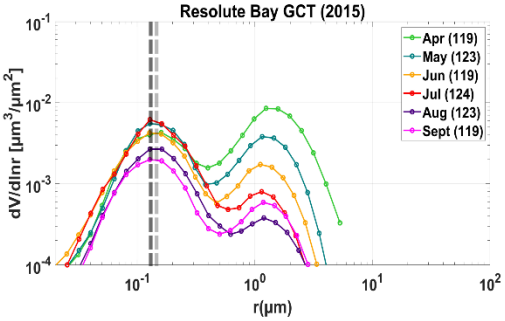
Resolute Bay GCT (2015)
Apr (119)
May (123)
Jun (119)
Jul (124)
Aug (123)
Sept (119)
dV/dlnr [μm³/μm²]
r(μm)

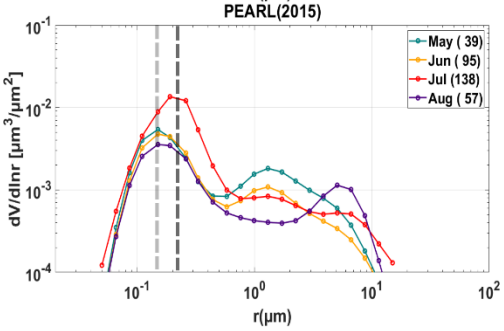
PEARL(2015)
May ( 39)
Jun ( 95)
Jul (138)
Aug ( 57)
dV/dlnr [μm³/μm²]
r(μm)

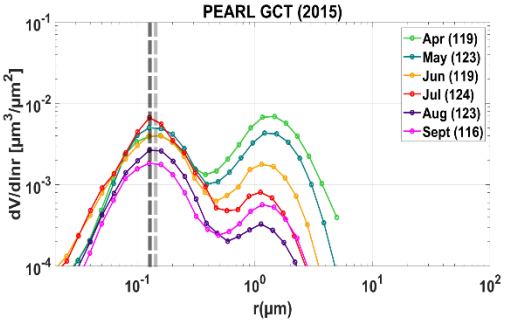
PEARL GCT (2015)
Apr (119)
May (123)
Jun (119)
Jul (124)
Aug (123)
Sept (116)
dV/dlnr [μm³/μm²]
r(μm)

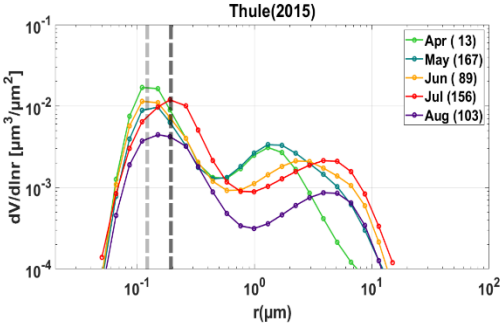
Thule(2015)
Apr ( 13)
May (167)
Jun ( 89)
Jul (156)
Aug (103)
dV/dlnr [μm³/μm²]
r(μm)

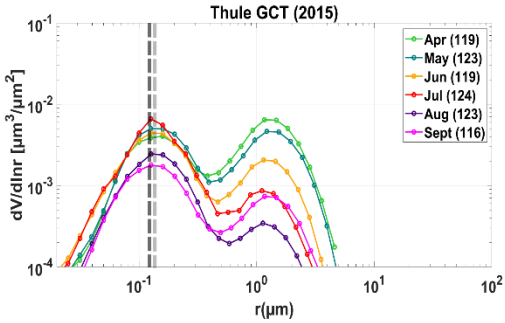
Thule GCT (2015)
Apr (119)
May (123)
Jun (119)
Jul (124)
Aug (123)
Sept (116)
dV/dlnr [μm³/μm²]
r(μm)

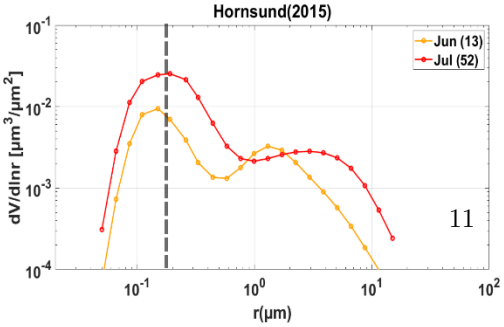
Hornsund(2015)
Jun (13)
Jul (52)
dV/dlnr [μm³/μm²]
r(μm)

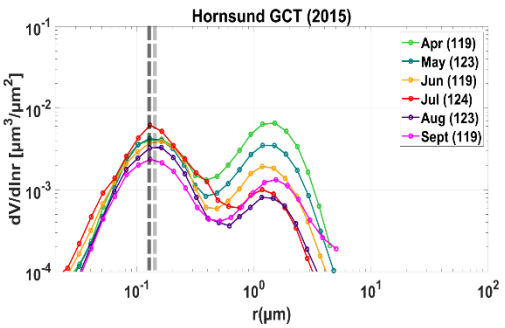
Hornsund GCT (2015)
Apr (119)
May (123)
Jun (119)
Jul (124)
Aug (123)
Sept (119)
dV/dlnr [μm³/μm²]
r(μm)

Figure 1 Monthly averaged volume PSDs of the five Arctic stations for 2015 AERONET retrievals (left column PSDs) and the GCT simulations (right column PSDs). The reader is referred to Table S1.1 and Table S1.2 of the supplementary material for specific bin center and bid edge values. The color of the curves corresponds to specific months where blue/green represents the spring months, orange/red the summer, and purple/bright pink the fall months. The total number of retrievals/points are shown in parentheses for each month. The vertical dashed grey and dark-grey lines indicate the spring and summer peaks respectively. In order to not burden Figure 1 with an excess of PSD details we purposely omitted the MYSP climatology PSDs of AeF. The reader is accordingly referred to that paper in order to make comparisons between the 2015 GCT and AERONET PSDs above with AeF's AERONET climatology.

## 4.2 AOD comparisons

### 4.2.1 FM AOD

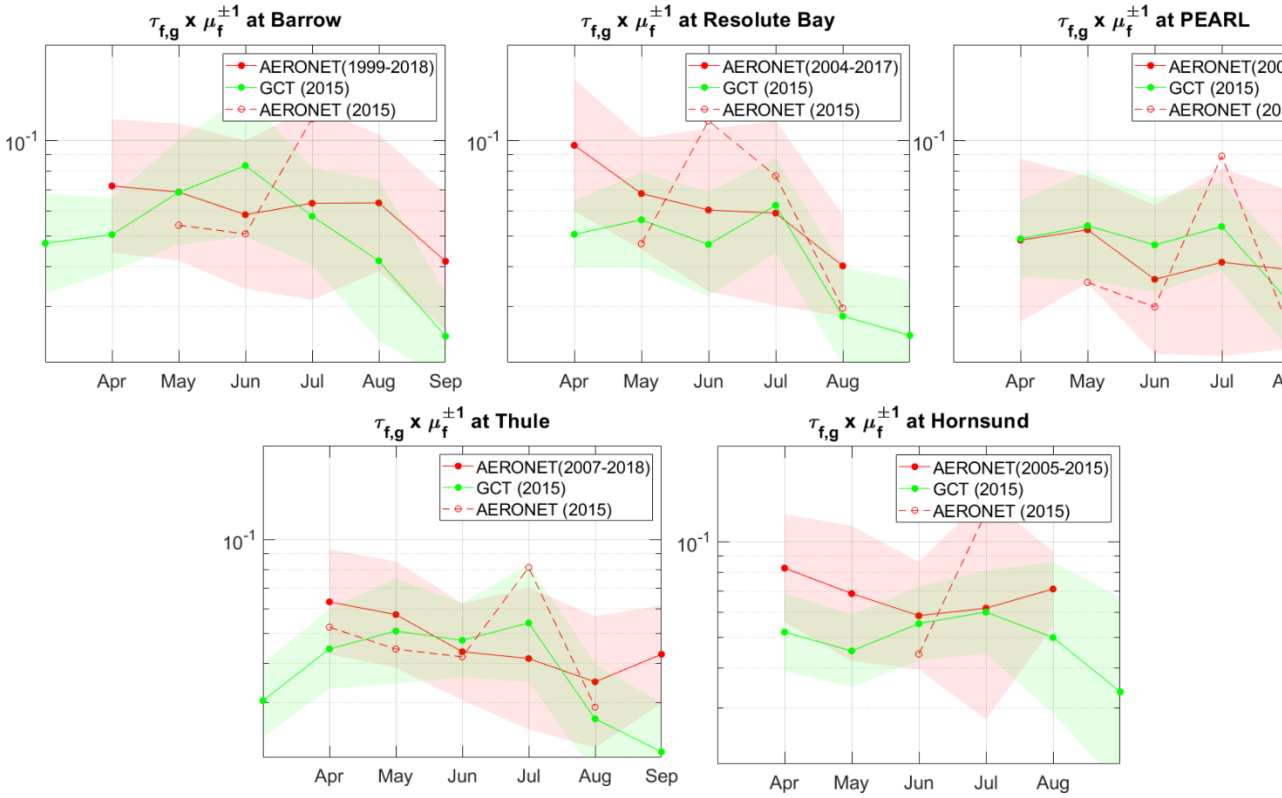


2 shows AeF's seasonal FM AOD climatology: the red solid-line shows the geometric means ($\tau_{f,g}$) while the pink envelope indicates the geometric standard deviation limits ($\tau_{f,g} \times \mu_f{}^{\pm 1}$). The analogous statistical parameters for the 2015 GCT simulations are shown, respectively, as a green solid line surrounded

by a green envelope. The cloud screening test (the impact of excluding GCT points for which the RH > 95%) showed that cloud screening had no significant effect. The impact of restricting GCT $\tau_{f,g}$ computations to times that were synchronous with AERONET retrieval times yielded differences of $<\sim 0.006$ (33%) for large-N months (N 20) and significantly larger differences of small-N months. In other words, GCT inevitably suffers from the same small-N statistical precariousness expected for the AERONET retrievals. It is worth noting that, non surprisingly, small N GCT values were generally associated with small-N AERONET retrievals.

The 2015 GCT results of Figure 2 are, with the exception of specific cases which we will explore below, reasonably close to the seasonal AeF variations ($\tau_{f,g}$values that are generally well within each other's standard deviation). Large-amplitude negative biases relative to the AeF climatology are most evident in the month of April for the GCT estimates at Barrow, Resolute Bay, Thule and Hornsund. The GCT seasonal simulations of Croft et al. (2016) underscored the (pan-Arctic, tropospheric) competition between accumulation (fine) mode (Arctic haze) increase in number density (largely due to northward transport of pollutants and Aitken mode condensation) and the decrease in accumulation mode lifetime due to wet deposition during the April-May spring transition (their Figure 8). The level of agreement between the GCT version chosen for their Figure 8 results (NEWSCAV+COAG) and surface measurements at Alert suggest that a modification of one or more of the three critical Figure 8 processes (with a focus on higher altitude impacts) would achieve a better match with the April $\tau_{f,g}$ results of AeF[9]. Large negative biases between GCT and the AeF climatology also occur at Barrow and Thule in September (the only sites for which there was a threshold value of 10 or more retrievals during that month). The GCT decrease is generally consistent with the (Figure 5, "NEWSCAV+COAG") August to September decrease of ("N20" and "N80") accumulation mode surface number density reported by Croft et al. (2016). AeF, on the other hand, noted the small-N precariousness of FM AOD statistics in the AERONET climatology during that month.

The July 2015 AERONET $\tau_{f,g}$retrievals (dashed red lines in Figure 2) are near the limits of or extend above the pink AeF envelope for all stations except Resolute Bay (which displays a $\tau_{f,g}$ peak in June[10]). Except for Barrow, the 2015 GCT $\tau_{f,g}$ values increase in July as well: the increases are inevitably sensitive at the event level to the dynamic (satellite-derived) GCT hot-spot emissions database but are considerably muted relative to the AERONET retrievals. Sioris et al. (2017) and Ranjbar et al. (2019) noted that the ( $\tau_f \sim 1$) peak during the 7-14 July 2015 period was an extreme smoke event at the PEARL site (with a confidence of $\sim 99.6\%$ if we employ the extreme-event statistics of the latter cita-

[9]although one would need to be wary of the precarious small-N results for Resolute Bay

[10]$\tau_f$ variations from the much higher temporal resolution AERONET-SDA product show a precipitous drop exactly from June 30 to July 1. This is an example of the precariousness of the assignment of $\tau_{f,g}$ values to a specific monthly bin in the presence of an extreme or near-extreme smoke event near the bin border between two months

tion). Movie S1 shows site by site $\tau_f$ temporal variations alongside animations of daily-averaged $\tau_f$ maps generated by GCT and NAAPS: the $\tau_f$ time series at all 5 sites show that GCT does not capture the higher frequency AERONET $\tau_f$ variations while NAAPS smoke AODs produce variations that respond in a similar higher frequency fashion to AERONET variations. The spatial animations and the synchronized temporal profiles support an argument that the difference in results is largely due to the AOD-driven features of NAAPS-RA coupled with differences in the spatial resolution of the two models. We note that the objective of the GCT simulations is to successfully model climatological-scale seasonal variations: the low frequency filtering of extremely high frequency events like the July 2015 smoke event is what we seek at the climatological scale.

In Section 4.3.1 below, we show that the GCT FM effective radii ($<r_{eff,f}>$) were significantly and systematically smaller than those of the AeF climatology and the 2015 AERONET retrievals (for all stations). The generally large-amplitude negative bias of GCT $\tau_{f,g}$estimates relative to the AERONET July 2015 retrievals are magnified in Figure S1 (solid-green curve) for all five stations. An approximate Mie transformation applied to the OC component of the GCT $\tau_{f,g}$ values (assuming a change in $r_{eff,f}$ from the GCT to the 2015 AERONET $<r_{eff,f}>$ values of Figure 6) yielded the dashed green ("enhanced") curve of Figure S1. The agreement of the enhanced curve relative to the 2015 AERONET values is significantly better (with greater differences for the small-N, large geometric standard deviation values of Barrow and Hornsund (c.f. the N values of Figure 1). This approximate argument supports the hypothesis of Section 4.3.1 that the GCT $<r_{eff,f}>$ underestimates of Figure 6 are largely attributable to shortcomings in estimating smoke (OC) particle size.

### 4.2.2 CM AOD

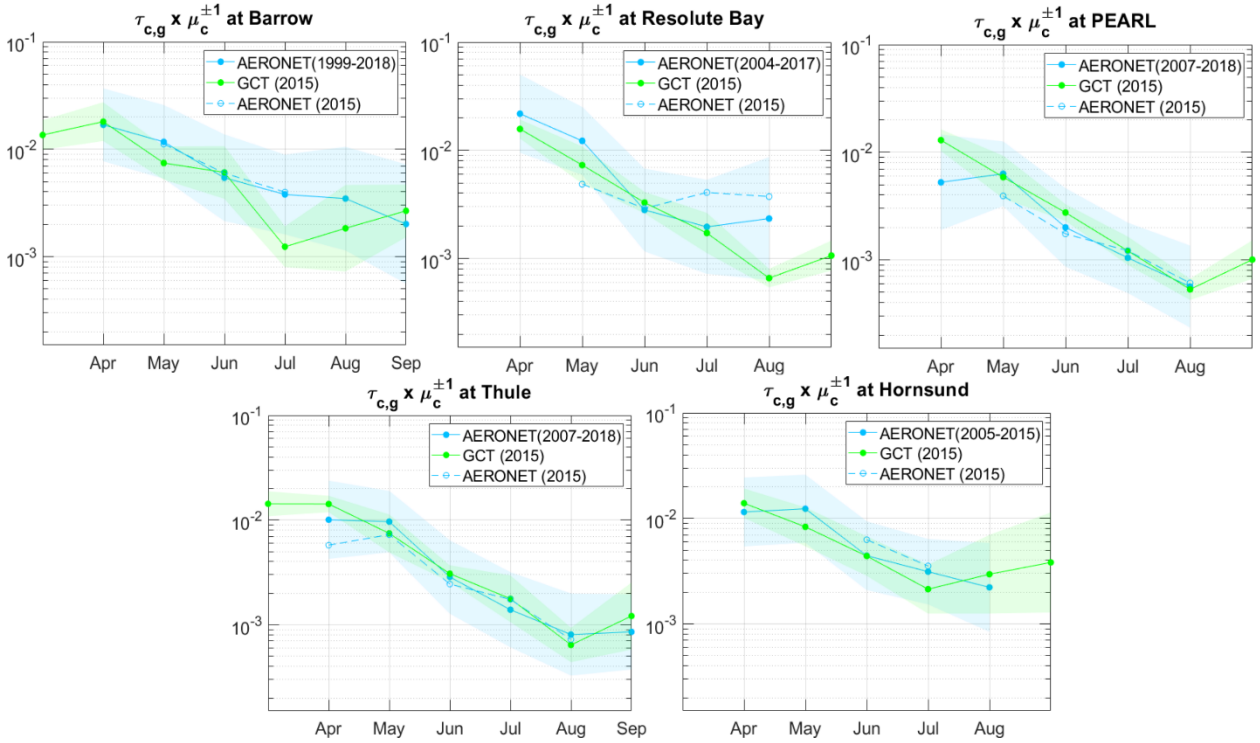


Figure 3 shows the 2015 GCT $\tau_{c,g}$ simulations and the 2015 AERONET retrievals superimposed on AeF's original climatology. The $\tau_{c,g}$ cloud screening impact was indentical to the $\tau_{f,g}$ tests (negligible). The impact of restricting GCT $\tau_{c,g}$ computations to AERONET-synchronous retrieval times yielded similar results to the fine mode analysis: differences of <~ 0.0004 (9%) for months with N 20.

The AeF and 2015 AERONET retrievals show a seasonal tendency that is similar to the GCT simulations: a general spring to summer decrease that AeF ascribed to the diminishing influence of Asian dust. The 2015 AERONET and GCT curves are usually well within the blue-coloured geometric standard deviation envelope of the AeF climatology: the notable differences relative to the 2015 retrievals occur for July at Barrow and August at Resolute Bay. The July Barrow results are likely influenced by small-N statistics (that actually impact all 2015 Barrow retrievals).

The GCT $\tau_{c,g}$ values show a significant fall (August or September) increase for all stations. This behavior is coherent with the increasing amplitude of the small-sized (1.2 to 1.5 µm radius peak) GCT modal feature described above (which we suggested was linked to the appearance of wind-induced sea-salt and/or dust particles). The optical influence of this modal feature extends to radii significantly

above those peak radii (extends well into radius regions where the modal feature has fallen well off from the peak) because of the associated increase in particle size: the (per particle) extinction cross section (effective optical extinction area) increases rapidly with increasing radius. The 2015 AERONET $\tau_{c,g}$ retrievals are largely insensitive to what is likely a real upturn in CM AOD while AeF noted a less rapid decrease of $\tau_{c,g}$ at Barrow, Resolute Bay and Hornsund. We note that the effective limit of August for (sufficiently high-N) AERONET inversions (even at the climatological scale) unfortunately inhibits our analysis of this GCT feature precisely when fall winds become stronger and more influential in generating substantial sea-salt and / or local dust events: the exploitation of moonphotometry (which already exists at several AERONET Arctic sites) and/or starphotometry[11] would help to better characterize the fall transition period.

### 4.2.3 FMF

The seasonal 2015 AERONET FMF results (Figure 4) largely follow the AeF climatology trend with the largest differences occurring in the early spring and late summer / fall when the weak number of retrievals has some impact (in spite of large $_{f,g}$ differences in July, the FMF difference is minimal because $_{f,g}$ is dominant over $_{c,g}$ and the FMF is, accordingly, a rather insensitive near-unity value). Similarly, the GCT 2015 FMF largely agrees with the FMF from the AeF climatology (the differences in Figure 5 are somewhat magnified by the relatively small extent of the FMF scale). The rough FMF similarity of all the curves is coherent with the reasoning reported in AeF: that the generally increasing FMF seasonal behaviour is driven by the generally decreasing seasonal amplitude of $_{c,g}$.

[11] currently located at Eureka and at Ny Alesund (some 240 km northwest of Hornsund)

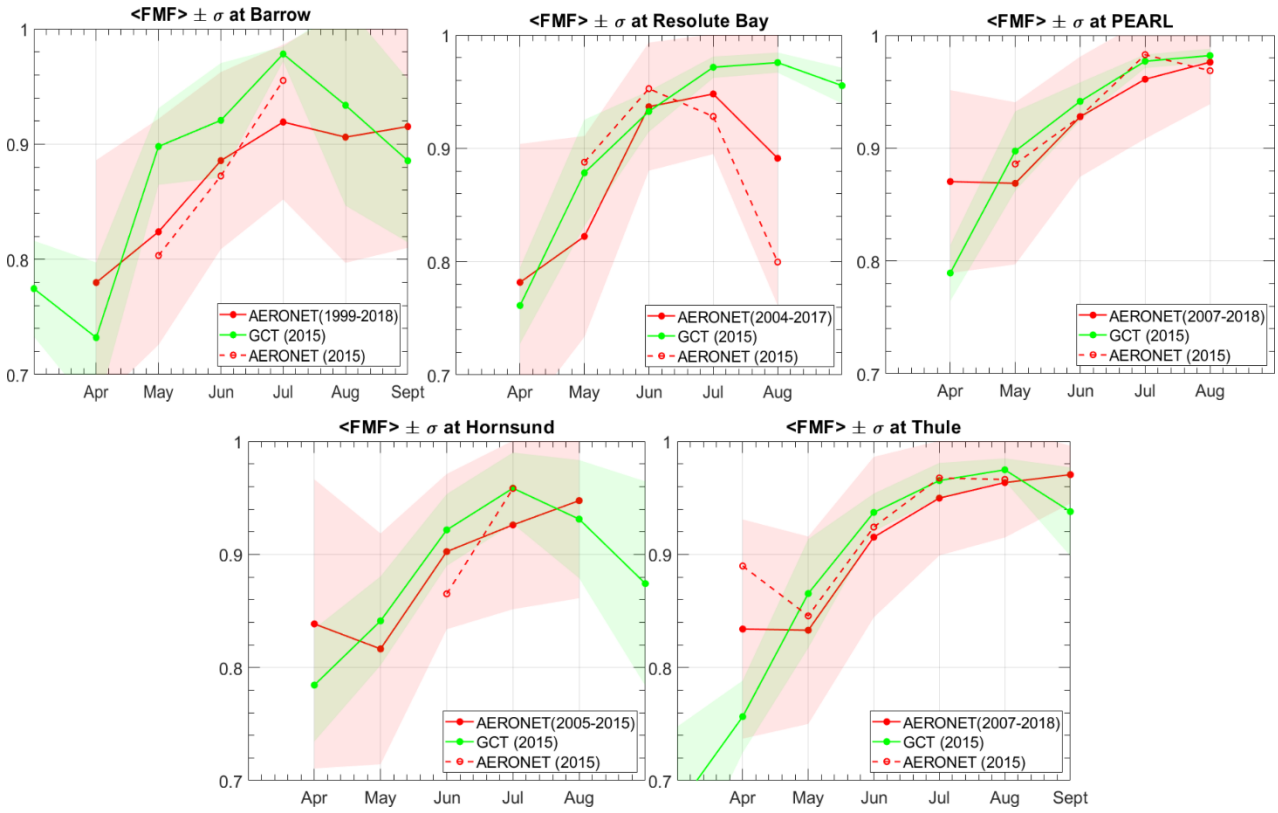


Figure 4 Seasonal FMF variation for all five Arctic stations. Same caption as Figure 2 (with appropriate changes to reflect that the statistics are represented by the arithmetic means and standard deviations of FMF).

## 4.3 Effective radius

Effective radius, being an intensive parameter in the context of FM or CM aerosols, is largely insensitive to the high (spatial and temporal) variations that characterize extensive parameters such as AOD. This robustness, as we will see in the following subsections, can provide clues to the nature of certain aerosol mechanisms or aerosol characteristics.

### 4.3.1 FM effective radius

Figure 5 shows the seasonal variation of monthly (arithmetically) averaged FM effective radii ($\langle r_{eff,f} \rangle$). AeF pointed out that the $>\sim 0.02$ µm seasonal increase in $\langle r_{eff,f} \rangle$ from spring to summer was likely due to the influence of large-particle FM smoke and the waning influence of FM Arctic haze. We supplied event-level evidence above on the extreme nature of the July 2015 smoke event. The GCT $\langle r_{eff,f} \rangle$ values of Figure 5 are biased negatively with respect to the AERONET

retrievals[12]. This is a bias that is significant relative to AeF and its pink envelope (except for Hornsund, the GCT mean is separated from the AeF mean by at least one AeF geometric standard deviation).

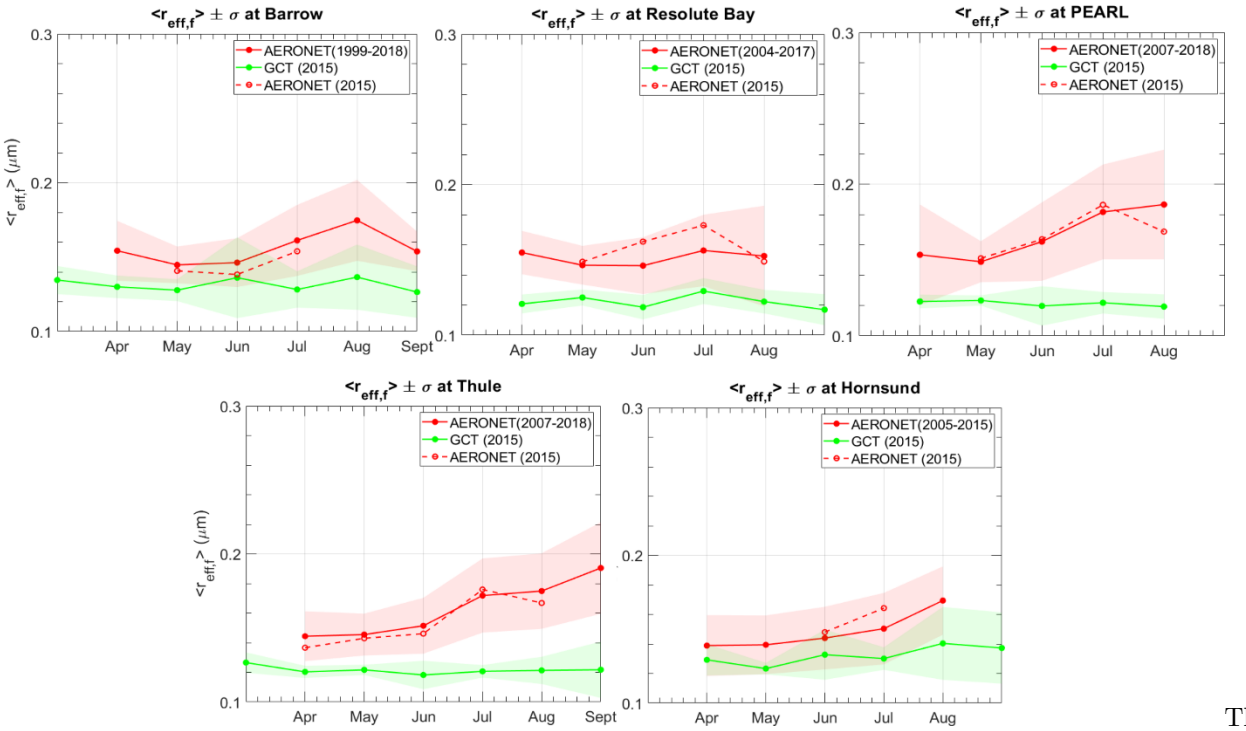


key influence on GCT underestimation relative to the AERONET July 2015 retrieval averages during the heavy smoke month of July 2015 is likely related to GCT underestimation of smoke particle size [13]. Ramnarine et al. (2019) showed that the coarseness of a GCT spatial resolution of 4° x 5° (the same as ours) resulted in a substantial underestimate of smoke particle size due to inadequate simulation of coagulation mechanisms (for a simulation corresponding to 24 hours of particle trajectory time). The diameter (and radius) of the number density PSD was ~ 60% larger with subgrid coagulation compared with a run without subgrid coagulation. The surface and volume PSDs and thus the effective radii likely go through a similar relative increase (see the log translatable PSD discussion of O'Neill et al., 2005), at least during smoke-impacted retrievals. In comparison, the increase from the GCT to

[12]biased negatively with respect to both AeF retrievals and the 2015 retrievals: in fact, the AeF climatology and 2015 retrievals are generally quite close. This is in keeping with the robustness of intensive parameters such as the FM effective radius

[13]We note that GCT also underestimates the springtime $\langle r_{eff,f} \rangle$ values by $<\sim 0.03$ μm. While we did not investigate the springtime difference in detail it is known that springtime smoke can be a factor of consequence that is even dominant in certain years (see the 2008 emissions and (PEARL) $\langle \tau_f \rangle$ variations shown in Figure 3 of Ranjbar et al.(2019).

AERONET $\langle r_{eff,f} \rangle$ values of Figure 6 was <~ 60%. In terms of the remote sensing relevance of AERONET $r_{eff,f}$ retrievals in actual smoke conditions, O'Neill et al., (2005) multi-station AERONET analysis amounted to an indirect validation of such retrievals: they showed a systematic $r_{eff,f}$ increase of 0.034 m per day of particle trajectory time for mid-latitude U.S. and Canadian AERONET stations during an extreme smoke event induced by intense fires near Hudson's Bay.

#### 4.3.2 CM effective radius

The arithmetic means of the CM effective radii ($\langle r_{eff,c} \rangle$) are plotted in Figure 6. The 2015 AERONET values are moderately close to the climatology curve (well within or near the edges of one AeF standard deviation). AeF attributed the spring to summer $\langle r_{eff,c} \rangle$ increase to the decreasing influence of the 1.3 µm (Asian dust) CM peak and the attendant increasing influence of the larger-radius 4 to 7 µm peak. GCT, as indicated above in the discussion of the 2015 PSDs (section 4.1), can not, given its bin-center upper limit of 4.5 µm, capture this second CM peak. However, we also noted that GCT did capture an amplitude increase and (not always) a moderate radius-position increase in the small-radius (1.2 to 1.5 µm) CM peak in August or September (with an attendant increase or lesser rate of seasonal decrease in $_{c,g}$). However, Figure 6 also shows a slow, seasonal GCT increase which is not confined to the months of August and September: while that seasonal increase is certainly influenced by the increase in amplitude and radius position of the small-radius GCT peak observed in Figure 1, it is complicated by the nature of the effective radius calculation: the minimum of the general CM GCT PSD (Figure 1) as well as the AERONET driven cut-off between the FM and CM regions are variable(see Section 3.2).

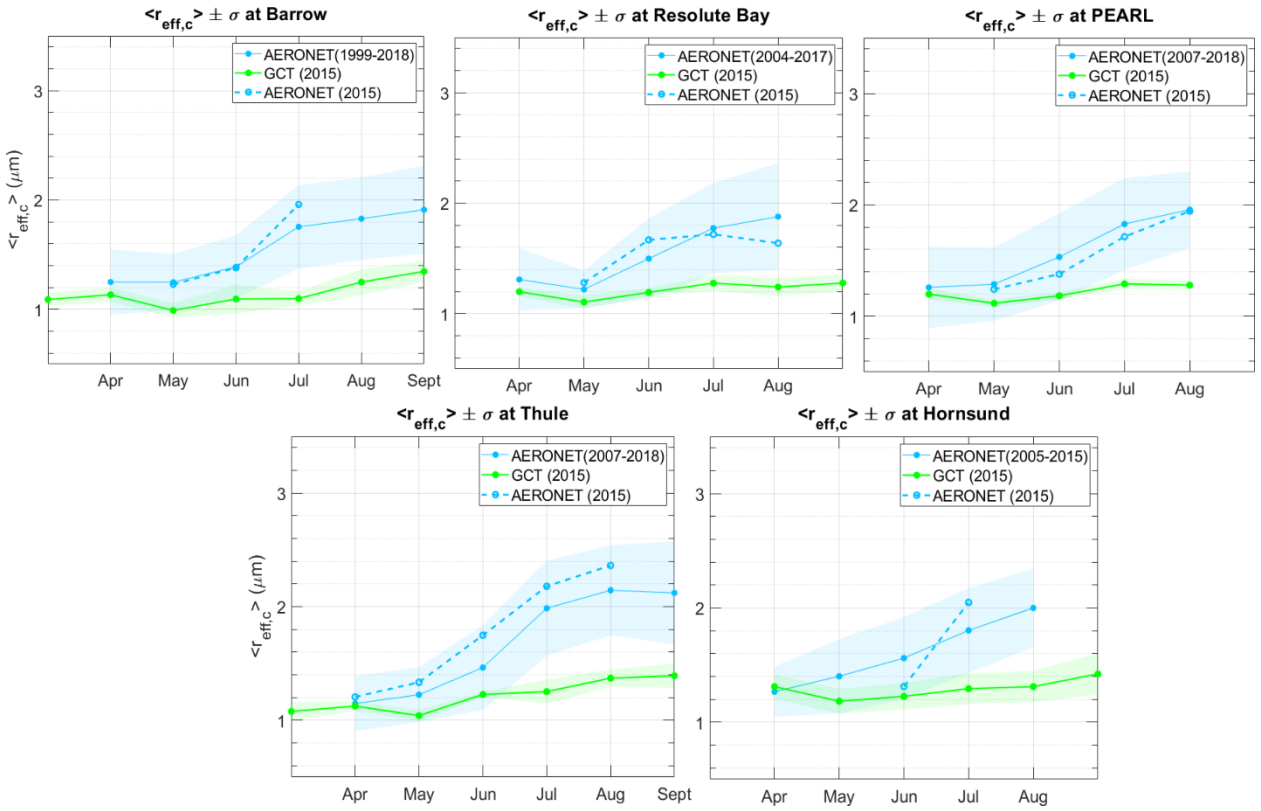


Figure 6 Seasonal <reff,c> variation for all five Arctic stations. Same caption as Figure 5 (with a colour change of red to blue for the AERONET retrievals).

# 5. Conclusions

GCT simulations of AERONET-inversion products during 2015 were compared with the AERONET-inversions products from the multi-year climatology of AeF and event-level (2015) AERONET products acquired over 5 stations in the North American and European Arctic. Monthly averaged (seasonal) analyses were carried out in the context of the spring to summer transition, the relatively stable summer period and the summer to early fall transition. A single year of GCT simulations was evaluated within the context of the geometrical/arithmetic means and geometrical/ arithmetic standard deviations of AeF's climatology as well as the 2015 AERONET retrieval parameters. This process enabled a better understanding of the robustness of seasonal variations derived from the AERONET retrievals and how well single-year GCT simulations could be employed to predict (climatological-scale) variations across the Arctic. When the 2015 AERONET retrievals departed excessively from the AeF climatology we sought to better understand the nature of these departures and how a single

year of GCT simulations could (i) help us understand the physical and optical dynamics of the AERONET (columnar) retrieval parameters at the event and climatological scale and (ii) understand any shortcomings of GCT in simulating those retrieval parameters.

GCT showed no significant spring to summer increase in the radius of the FM peak: an insensitivity that was likely due to a general GCT underestimation of smoke particle size. The small-sized (springtime) GCT CM peak feature (1.1 to 1.5 µm radius peak) is roughly coherent with the 1.3 µm (Asian dust) peak reported by AeF. The GCT PSDs did not appear to capture any element of the larger-sized (4 to 7 µm CM peaking) reported by AeF (who suggested that this was more likely to be due to local dust). The small-sized GCT CM peak feature tended to rapidly decrease in amplitude as the season progressed (a tendency that was coherent with the amplitude decrease of AeF's 1.3 µm peak). However, this decreasing-amplitude trend went through a reversal with amplitude increases at all stations in August and/or September. Those increases might have physical links to AeF's larger-sized (4 to 7 µm) CM peak feature in the fall months: i.e., similar types of CM particles where the GCT variations are restricted to lower radius sizes by the constraints of the PSD source functions (see Gong, 2003 and Zhang et al., 2013) for sea-salt and dust respectively) combined with the upper-bin limitation of 4.5 µm.

The 2015 GCT $\tau_{f,g}$estimates were generally close to the seasonal AeF variations. GCT springtime biases of large amplitude (relative to the April AeF climatology) were thought to be linked to the simulated nature of the competition between accumulation FM increase in number density (Arctic haze) and its decrease in lifetime due to wet deposition. The July 2015 AERONET $\tau_{f,g}$retrievals were, in general, significantly larger than the AeF climatology (as were the GCT simulations but considerably muted relative to the 2015 retrievals). GCT did not capture the higher frequency AERONET $\tau_f$ variations while the smoke AODs predicted by the NAAPS model were similar to the high frequency AERONET variations. This was likely attributable to the higher temporal resolution of NAAPS biomass burning emissions, the employment of assimilated AODs (and their general higher spatial resolution).

The GCT simulations and the 2015 AERONET $\tau_{c,g}$retrievals showed a spring to summer decrease that was similar to the tendency that AeF ascribed to the diminishing influence of Asian dust. GCT showed a systematic late summer / fall (August or September) increase at all stations. This behavior was coherent with the increasing amplitude and/or radius position of the small-sized CM GCT peaks observed in the PSD analysis. The GCT FMF simulations largely followed AeF's seasonal trend of increasing FMF (a trend that was driven in both cases by the decreasing seasonal amplitude of $_{c,g}$).

GCT $\langle r_{eff,f} \rangle$ values were underestimated relative to both AeF and the 2015 AERONET retrievals. It was argued that inadequate simulation of sub-grid coagulation smoke particles was a plausible reason for the underestimation and

that an $<r_{eff,f}>$ increase from the GCT to AERONET values for the heavy smoke month of July 2015 (for all stations) increased the GCT $\tau_{f,g}$ values to levels which were close to the AERONET $\tau_{f,g}$ retrievals. The 2015 AERONET $\langle r_{eff,c} \rangle$ values were generally close to the AeF climatology curve (a variation ascribed to the decreasing influence of the Asian dust CM peak and the increasing influence of the larger-radius 4 to 7 µm peak). Because GCT only captured the lesser amplitude increase in the small-sized CM peak in August / September, its seasonal increase corresponded to a significantly lesser rate than the AERONET retrievals.

The seasonal GCT (PSD, FM and CM) results reported in this paper are generally robust and sufficiently accurate to have a significant accuracy influence on aerosol, aerosol-cloud-interaction and radiative forcing models over the Arctic. A knowledge of the seasonal variation of smoke and dust optical depths will have important consequences on the simulations of the deposition impacts of absorbing aerosols on snow reflectance. The prediction of both extensive and intensive CM and FM parameters, as well as key features of the PSD, represent an advancement over the use of classical extensive and semi-extensive columnar parameters of AOD and (regression) Angstrom exponent that tend to be the source of evaluation of the opto-physical packages of current aerosol-cloud models.

## Acknowledgments

We would like to express our gratitude to NSERC (National Sciences and Engineering Research Council) of Canada for CCAR funding via the NETCARE and PAHA projects and the DG funding of O'Neill as well as the CSA (Canadian Space Agency) for the SACIA (Signatures of Aerosol-Cloud Interaction over the Arctic) project funding (ESS-DA program). The support of AEROCAN (Environment Change and Climate Change Canada), AERONET (NASA/GSFC), and the operation staff at the five sites whose retrievals we employed are gratefully acknowledged. The resource support of Compute Canada/Calcul Quebec was also greatly appreciated. We thank the site-PIs for their effort in establishing and maintaining the AERONET/AEROCAN sites: Brent Holben for Thule and Hornsund, Grzegorz Karasinksi and Piotr Glowacki for Hornsund, and Rick Wagener, Laurie Gregory, and Lynn Ma for Barrow, and Vitali Fioletov for Resolute Bay, Eureka., Data used in this study is available at the AERONET website.

## Symbols and Acronym Glossary

| | |
|---|---|
| AeF | Aboelfetouh et al. (2020) |
| AEROCAN | Federated Canadian subnetwork of AERONET run by Environment and Climate Change Cana |
| AERONET | Aerosol Robotic Network: World-wide NASA network of combined sunphotometer / sky-scann |
| AOD | Aerosol optical depth: The community uses "AOD" to represent anything from nominal aeroso |
| BC | Black Carbon |
| CM | coarse mode (supermicron particle radius) |
| CTM | Chemistry Transport Model |
| FM | fine mode (submicron particle radius) |
| FMF | fine mode fraction |
| GC | GEOS(Goddard Earth Observing System)-Chem |
| $m_p$ | Complex refractive index (where p=r for the real part & p=i for the imaginary). |
| MERRA-2 | Modern-Era Retrospective analysis for Research and Application, Version 2 |
| MYSP | Multi-year sampling Period (different for each station) for which we acquired AERONET/Dub |
| NAAPS | Navy Aerosol Analysis and Prediction system |
| NAAPS-RA | NAAPS Reanalysis |
| NETCARE | Network on Climate and Aerosols: Addressing key uncertainties in Remote Canadian Environn |
| NSERC | Natural Sciences and Engineering Research Council of Canada |
| OC | Organic carbon |
| PEARL | Polar Environmental Atmospheric Research Laboratory |
| PSD | particle size distribution (precisely, the volume particle size distribution) |
| RH | Relative humidity |
| SS | Sea-salt |
| GCT | GEOS-Chem-TOMAS (TwO Moment Aerosol Sectional) |
| x | x = f or c (fine mode or coarse mode) |
| $\langle \mathbf{r_{eff,x}} \rangle$ | Arithmetic mean of the effective radii for monthly averaging bins |
| $_{x})$ | Arithmetic standard deviation for monthly averaging bins for AODs |
| $\mathbf{r_{eff,x}})$ | Arithmetic standard deviation for monthly averaging bins for effective radii |
| $_{\mathbf{x,g}}$ | Geometric mean for monthly averaging bins. $\tau_{x,g} = 10^{\log \tau_x >}$ (see Table 1 of O'Neill et al., 200 |
| $\mu_x$ | Geometric standard deviation for monthly averaging bins. $\mu_x = 10^{\sigma(\log \tau_x)}$ (see Table 1 of O'Ne |

# References

AboEl-Fetouh, Y., O'Neill, N. T., Ranjbar, K., Hesaraki, S., Abboud, I., & Sobolewski, P. S. (2020). Climatological-Scale Analysis of Intensive and Semi-intensive Aerosol Parameters Derived From AERONET Retrievals Over the Arctic. *Journal of Geophysical Research: Atmospheres*, *125*(10), 1–19. https://doi.org/10.1029/2019JD031569Adams, P. J., & Seinfeld, J. H. (2002). Predicting global aerosol size distributions in general circulation models. *Journal of Geophysical Research Atmospheres*, *107*(19), 1–23. https://doi.org/10.1029/2001JD001010Bohren, C. F., & Huffman, D. R. (2004). *Absorption and Scattering of Light by Small Particles* (First publ). Weinheim: WILEY-VCH Verlag GmbH & Co. KGaA. https://doi.org/10.1002/9783527618156Bond, T. C., & Bergstrom, R. W.

(2006). Aerosol Science and Technology Light Absorption by Carbonaceous Particles: An Investigative Review Light Absorption by Carbonaceous Particles: An Investigative Review. *Aerosol Science and Technology*, *40*(1), 27–67. https://doi.org/10.1080/02786820500421521Boucher, O., Randall, D., Artaxo, P., Bretherton, C., Feingold, G., Forster, P., et al. (2013). *Clouds and Aerosols. In: Climate Change 2013: The Physical Science Basis. Contribution of Working Group I to the Fifth Assessment Report of the Intergovernmental Panel on Climate Change [Stocker, T.F., D. Qin, G.-K. Plattner, M. Tignor, S.K. Allen, J. Bos.* Cambridge University Press, Cambridge, United Kingdom and New York, NY, USA. Retrieved from https://www.ipcc.ch/pdf/assessment-report/ar5/wg1/WG1AR5_Chapter07_FINAL.pdfBreider, T. J., Mickley, L. J., Jacob, D. J., Wang, Q., Fisher, J. a., Chang, R. Y.-W., & Alexander, B. (2014). Annual distributions and sources of Arctic aerosol components, aerosol optical depth, and aerosol absorption. *Journal of Geophysical Research: Atmospheres*, *119*(7), 4107–4124. https://doi.org/10.1002/2013JD020996Croft, B., Wentworth, G. R., Martin, R. V., Leaitch, W. R., Murphy, J. G., Murphy, B. N., et al. (2016). Contribution of Arctic seabird-colony ammonia to atmospheric particles and cloud-albedo radiative effect. *Nature Communications*, *7*, 1–10. https://doi.org/10.1038/ncomms13444Croft, Betty, Martin, R. V, Leaitch, W. R., Tunved, P., Breider, T. J., D'andrea, S. D., & Pierce, J. R. (2016). Processes controlling the annual cycle of Arctic aerosol number and size distributions. *Atmos. Chem. Phys*, *16*, 3665–3682. https://doi.org/10.5194/acp-16-3665-2016Croft, Betty, Martin, R. V., Richard Leaitch, W., Burkart, J., Chang, R. Y. W., Collins, D. B., et al. (2019). Arctic marine secondary organic aerosol contributes significantly to summertime particle size distributions in the Canadian Arctic Archipelago. *Atmospheric Chemistry and Physics*, *19*(5), 2787–2812. https://doi.org/10.5194/acp-19-2787-2019Curci, G., Hogrefe, C., Bianconi, R., Im, U., Balzarini, A., Baró, R., et al. (2015). Uncertainties of simulated aerosol optical properties induced by assumptions on aerosol physical and chemical properties: An AQMEII-2 perspective. *Atmospheric Environment*, *115*, 541–552. https://doi.org/10.1016/j.atmosenv.2014.09.009Dick, W. D., Saxena, P., & Mcmurry, P. H. (2000). Estimation of water uptake by organic compounds in submicron aerosols measured during the Southeastern Aerosol and Visibility Study. *Journal of Geophysical Research*, *105*(D1), 1471–1479. https://doi.org/10.1029/1999JD901001Dubovik, O., & King, M. D. (2000). A flexible inversion algorithm for retrieval of aerosol optical properties from Sun and sky radiance measurements. *Journal of Geophysical Research: Atmospheres*, *105*(D16), 20673–20696. https://doi.org/10.1029/2000JD900282Dubovik, O., Holben, B., Eck, T. F., Smirnov, A., Kaufman, Y. J., King, M. D., et al. (2002). Variability of Absorption and Optical Properties of Key Aerosol Types Observed in Worldwide Locations. *Journal of the Atmospheric Sciences*, *59*(3), 590–608. https://doi.org/10.1175/1520-0469(2002)059<0590:VOAAOP>2.0.CO;2Gelaro, R., McCarty, W., Suárez, M. J., Todling, R., Molod, A., Takacs, L., et al. (2017). The modern-era retrospective analysis for research and applications, version 2 (MERRA-2). *Journal of Climate*, *30*(14), 5419–5454. https://doi.org/10.1175/JCLI-D-16-0758.1Gong,

S. L. (2003). A parameterization of sea-salt aerosol source function for sub- and super-micron particles, *17*(4), 1–7. https://doi.org/10.1029/2003GB002079Hesaraki, S., Neill, N. T. O., Lesins, G., Saha, A., Randall, V., Fioletov, V. E., et al. (2017). Comparisons of a Chemical Transport Model with a Four-Year ( April to September ) Analysis of Fine- and Coarse-Mode Aerosol Optical Depth Retrievals Over the Canadian Arctic. *Atmosphere-Ocean*, *55*(4–5), 213–229. https://doi.org/10.1080/07055900.2017.1356263Hirdman, D., Burkhart, J. F., Sodemann, H., Eckhardt, S., Jefferson, A., Quinn, P. K., et al. (2010). Long-term trends of black carbon and sulphate aerosol in the Arctic: Changes in atmospheric transport and source region emissions. *Atmospheric Chemistry and Physics*, *10*(19), 9351–9368. https://doi.org/10.5194/acp-10-9351-2010Kodros, J. K., & Pierce, J. R. (2017). Important global and regional differences in aerosol cloud-albedo effect estimates between simulations with and without prognostic aerosol microphysics. *Journal of Geophysical Research: Atmospheres*, *122*(7), 4003–4018. https://doi.org/10.1002/2016JD025886Kodros, J. K., Hanna, S. J., Bertram, A. K., Leaitch, W. R., Schulz, H., Herber, A. B., et al. (2018). Size-resolved mixing state of black carbon in the Canadian high Arctic and implications for simulated direct radiative effect. *Atmospheric Chemistry and Physics*, *18*(15), 11345–11361. https://doi.org/10.5194/acp-18-11345-2018Leaitch, R. R., Kodros, J. K., Willis, M. D., Hanna, S., Schulz, H., Andrews, E., et al. (2020). Vertical profiles of light absorption and scattering associated with black carbon particle fractions in the springtime Arctic above 79°N. *Atmospheric Chemistry and Physics*, *20*(17), 10545–10563. https://doi.org/10.5194/acp-20-10545-2020Lesins, G., Chylek, P., & Lohmann, U. (2002). A study of internal and external mixing scenarios and its effect on aerosol optical properties and direct radiative forcing, *107*.O'Neill, N. T., Eck, T.F., Smirnov, A, Holben, B.N., and Thulasiraman, S. (2003). Spectral discrimination of coarse and fine mode optical depth. *Journal of Geophysical Research*, *108*(D17), 1–15. https://doi.org/10.1029/2002JD002975O'Neill, N. T., Thulasiraman, S., Eck, T. F., & Reid, J. S. (2005). Robust optical features of fine mode size distributions: Application to the Qu??bec smoke event of 2002. *Journal of Geophysical Research D: Atmospheres*, *110*(11), 1–16. https://doi.org/10.1029/2004JD005157Ramnarine, E., Kodros, J. K., Hodshire, A. L., Lonsdale, C. R., Alvarado, M. J., & Pierce, J. R. (2019). Effects of near-source coagulation of biomass burning aerosols on global predictions of aerosol size distributions and implications for aerosol radiative effects. *Atmospheric Chemistry and Physics*, *19*(9), 6561–6577. https://doi.org/10.5194/acp-19-6561-2019Ranjbar, K., O'Neill, N. T., AboEl-fetouh, Y., Lutsch, E., Lesins, G., McCullough, E., et al. (2019). Extreme smoke event over the high Arctic. *Submitted to Atmospheric Environment*.Sayer, A. M., & Knobelspiesse, K. D. (2019). How should we aggregate data ? Methods accounting for the numerical distributions , with an assessment of aerosol optical depth. *Atmospheric Chemistry and Physics, Discussions*, (July), 1–36.Schmale, J., Zieger, P., & Ekman, A. M. L. (2021). Aerosols in current and future Arctic climate. *Nature Climate Change*, *11*(February). https://doi.org/10.1038/s41558-020-00969-5Sinyuk, A., Holben, B. N., Eck, T. F., Giles, D. M., Slutsker, I., Korkin,

S., et al. (2020). The AERONET Version 3 aerosol retrieval algorithm, associated uncertainties and comparisons to Version 2. *Atmos. Meas. Tech*, *13*, 3375–3411. https://doi.org/10.5194/amt-13-3375-2020Sirois, A., & Barrie, L. A. (1999). Arctic lower tropospheric aerosol trends and composition at Alert , Canada : 1980-1995. *Journal of Geophysical Research*, *104*(D9), 11599–11618. https://doi.org/https://doi.org/10.1029/1999JD900077Tang, I. N. (1996). Chemical and size effects of hygroscopic aerosols on light scattering coefficients. *Journal of Geophysical Research*, *101*(D14), 19245. https://doi.org/10.1029/96JD03003Tegen, I., & Fung, I. (1994). Modeling of mineral dust in the atmosphere: Sources, transport, and optical thickness. *Journal of Geophysical Research*, *99*(D11), 22,897-22,914. https://doi.org/10.1029/94JD01928Trivitayanurak, W., Adams, P. J., Spracklen, D. V., & Carslaw, K. S. (2008). Tropospheric aerosol microphysics simulation with assimilated meteorology: model description and intermodel comparison. *Atmospheric Chemistry and Physics Discussions*, *7*(5), 14369–14411. https://doi.org/10.5194/acpd-7-14369-2007Zhang, X., Huang, Y., Rao, R., & Wang, Z. (2013). Retrieval of effective complex refractive index from intensive measurements of characteristics of ambient aerosols in the boundary layer. *Optics Express*, *21*(15), 17849–62. https://doi.org/10.1364/OE.21.017849